Journal of
Materials Chemistry C

Materials for optical, magnetic and electronic devices

## Accepted Manuscript

This article can be cited before page numbers have been issued, to do this please use: C. Akyol, M. Baskurt and H. Sahin, *J. Mater. Chem. C*, 2020, DOI: 10.1039/D0TC03062G.

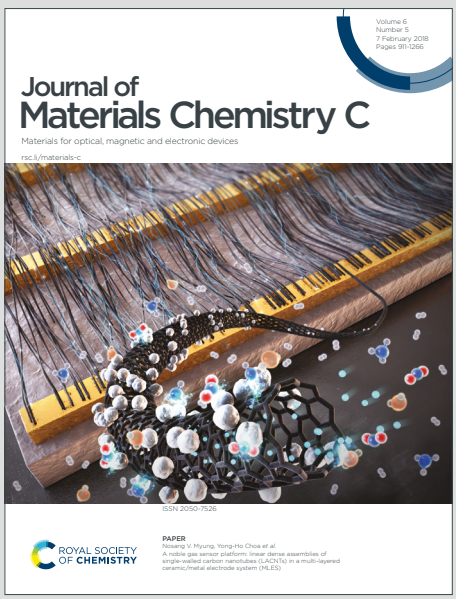




ROYAL SOCIETY OF CHEMISTRY

rsc.li/materials-c

View Article Online
DOI: 10.1039/D0TC03062G

Journal Name

ARTICLE TYPE

Cite this: DOI: 00.0000/xxxxxxxxxx

# Novel Ultra-Thin Two-Dimensional Structures of Strontium Chloride†

Cansu Akyol,[a] Mehmet Baskurt,[a] and Hasan Sahin*[ab]

Received Date
Accepted Date

DOI: 00.0000/xxxxxxxxxx

By performing density functional theory-based calculations, possible stable ultra-thin crystal structures of $SrCl_2$ are investigated. Phonon calculations reveal that, among possible crystal structures, three different phases; namely 1H, 1T, and Square, are dynamically stable. In addition, *ab initio* molecular dynamics calculations show that these three phases are thermally stable up to well above room temperature. Another important stability factor of crystals, the chemical inertness against abundant molecules in the atmosphere such as $N_2$, $O_2$, $H_2O$, and $CO_2$ is also investigated. The analysis show that $SrCl_2$ single-layers are chemically stable against these molecules. Moreover, it is determined that in contact with $H_2O$ and $CO_2$, ultra-thin $SrCl_2$ sheets display unique electronic features, allowing them to be used in sensing applications. It is also shown that single layers of $SrCl_2$ crystals, all having wide electronic band gap, can form type-I and type-II vertical van der Waals heterostructures with well-known 2D materials such as $MoS_2$, $WSe_2$, *h*-BN.

## 1 Introduction

Alkaline earth halides with their high ionic conductivity and stability hold promise for practical applications in the wide range of fields.[1] Also, they are promising building blocks for upcoming nanotechnology products. The fusion temperatures of alkaline earth halides are of great importance for the interpretation of the phase balance and electrical conductivity measurements in metal-metal halides.[2] As a well-known Grignard reagent,[3,4] $MgBr_2$ is used for removal of silyl protecting groups and catalysis in diastereoselective hydrogenation reactions of alkenes.[5,6] In addition, $CaF_2$ is used in various range of applications in such as dentistry, diode pump, ceramic lasers and insulating layer in transistors.[7–14] Bulk $BaF_2$, with its transparent crystal structure from UV to IR regions, reported as a useful material for infrared spectroscopy and medical imaging systems.[15–18] Another member of the family, $SrCl_2$, has found applications in dentistry and biology.[19–22]

Demonstrating efficient results in variety of fields in its bulk form, $SrCl_2$ has also gained interest in low dimensional form. Thin layer $SrCl_2$ electrolyte was reported to be efficient sensor for measuring the partial pressure of hydrogen.[23] Using $SrCl_2$ thin films in design of a chemisorption composite was shown to improve overall adsorption efficiency.[24] In addition, it was observed that thin films of $SrCl_2$ can also play important role in solar cell applications. Environmentally friendly $SrCl_2$ is used as an alternative to $CdCl_2$ in thin film solar cells which improves the efficiency of the cell.[25] Moreover, it was also shown that passivation of perovskite thin film solar cells with spin-coated $SrCl_2$ layer enhances the power conversion efficiency over 21%.[26]

Nowadays, as a result of rapid advances in experimental studies, dimensional reduction of materials can be done even down to few-atom thickness. Following the discovery of graphene,[27,28] synthesis of novel ultra-thin metals (borophene, $TaS_2$),[29,30] semiconductors ($MoS_2$, $WSe_2$ $ReS_2$, Xenes),[31–39] insulators (*h*-BN, $CaF_2$, $CaCl_2$, $CaBr_2$, $CaI_2$),[40–43] and ferromagnetic crystals ($CrI_3$, $Cr_2Ge_2Te_6$, $VI_3$, $MnSe_2$)[44–48] have been reported. It has also recently reported that doped monolayers of $HfSe_2$, $C_3N$ are good candidates for sensing applications.[49,50] Although the macroscale forms have been studied previously, to the best of our knowledge, ultra-thin forms of $SrCl_2$ crystals have not yet been reported.

In this study, motivated by recent advances in synthesis of ultra-thin graphene-like structures, possible atomically-thin 2D crystal structures of $SrCl_2$ are investigated. In section 2 detailed explanation about the computational methodology is given. Structural properties of 1H, 1T, and Square phases of $SrCl_2$ crystals are given in the section 3. Vibrational, thermal and chemical stabilities of three phases are examined in the section 4. In the section 5, electronic properties and band alignments of the possible vertical heterostructures of the stable $SrCl_2$ single-layers are investigated. Finally, our results are concluded in section 6.

[a] *Department of Photonics, Izmir Institute of Technology, 35430, Izmir, Turkey. E-mail: hasansahin@iyte.edu.tr*
[b] *ICTP-ECAR Eurasian Center for Advanced Research, Izmir Institute of Technology, 35430, Izmir, Turkey*

View Article Online
DOI: 10.1039/D0TC03062G





## 2 Computational Methodology

In this study investigating the structural, vibrational and electronic properties of single-layer 1H, 1T and Square $SrCl_2$ crystals performed using density functional theory (DFT) with embodied in the Vienna *ab-initio* Simulation Package (VASP)[51,52]. The energy of exchange and correlation was evaluated by using Perdew-Burke-Ernzerhof (PBE) parameters with expanded crystal wave functions on the basis of plane wave set using periodic boundary conditions in generalized gradient approximation (GGA).[53] Plane-wave projector augmented-wave (PAW) was used with the projector to accurately represent valence-core interactions.[54] The charge transfer between atoms determined by Bader technique.[55]

A plane wave cutoff of 500 eV was used for $SrCl_2$ phases. Convergence criterion of $10^{-4}$ eV and $10^{-5}$ eV were taken between individual ionic and electronic steps, respectively. For structural and electronic properties, 0.05 eV Gaussian smearing was used. The vacuum space was taken at least 15 Å, in order to prevent any interaction between adjacent layers. Geometric relaxations were allowed until the pressures became lesser than 1kB in all directions. The cohesive energies for per formula was calculated using Eq. 1.

$$E_{coh} = \sum_a n_a E_a - E_{system} \quad (1)$$

Vibrational properties are calculated using the small displacement method implemented within PHON and PHONOPY code.[56,57] For the molecular dynamics (MD) simulations NVE ensemble is used. The k-point sampling is chosen as 3×3×1 for 4×4×1 supercell. Time step of 2 fs is used in the dynamical simulation. The temperature is increased from 0 K to 2000 K in total simulation time of 2 ps.

## 3 Structural Properties of Possible $SrCl_2$ Structures

Bulk strontium chloride crystallizes in a fluorite-type structure and its ionic arrangement can be described as face-centered cubic. Single-layer structures of 1H, 1T, and Square phases can be obtained by truncation of bulk $SrCl_2$. In this study, possible single-layer structures of $SrCl_2$ in 1H, 1T, and Square phases are investigated. Total energy differences and optimized structures of 1H, 1T and Square phases of $SrCl_2$ are presented in Figure 1. Within its single-layers, 1T-$SrCl_2$ structure has a relatively lower cohesive energy (0.35 eV) with respect to the Square phase while Square phase has a lower cohesive energy (0.04 eV) with respect to the 1H phase. Lattice parameters of the optimized crystal structures of primitive unit cell of bulk, 1H, 1T and Square phases are 4.99, 4.18, 4.42 and 3.70 , respectively. Sr–Cl bond length varies between 2.92–3.08 Å where 1T has the shortest, Square phase has the longest bond length which indicates the cohesion between Sr and Cl atoms are the strongest in 1T phase and weakest in Square phase. These results are supported by the cohesive energies of $SrCl_2$ single layers, as given in Table 1. Moreover, Bader analysis reveals that the bonds between Sr and Cl atoms has ionic character in all single-layer $SrCl_2$ structures formed by 0.8 $e^-$ charge donation from Sr to Cl atoms as in the bulk form.

Furthermore, elastic properties for these three novel phases of $SrCl_2$ are calculated. In-plane stiffness values of 1H, 1T, and Square phases are respectively 20, 20 and 51 N/m that makes them softer materials compared to in-demand materials like graphene(330 N/m), $MoS_2$(122 N/m) and *h*-BN(273 N/m). Poisson ratio of the 1H phase is 0.47 which is closer to silicene (0.41) and germenene (0.42). Poisson ratio of 1T phase is 0.24 and this value is closer to values of various materials such as *h*-BN (0.22) and $MoS_2$ (0.26).[58] Among the possible single layer structures of $SrCl_2$ Poisson ratio of the Square phase is found to be the smallest one (0.05) indicating its structural robustness against the compressive and tensile uniaxial strain. Further investigations on the structural stability of phases of single layer $SrCl_2$, obtained from total energy optimization calculations, are performed in the following chapters.

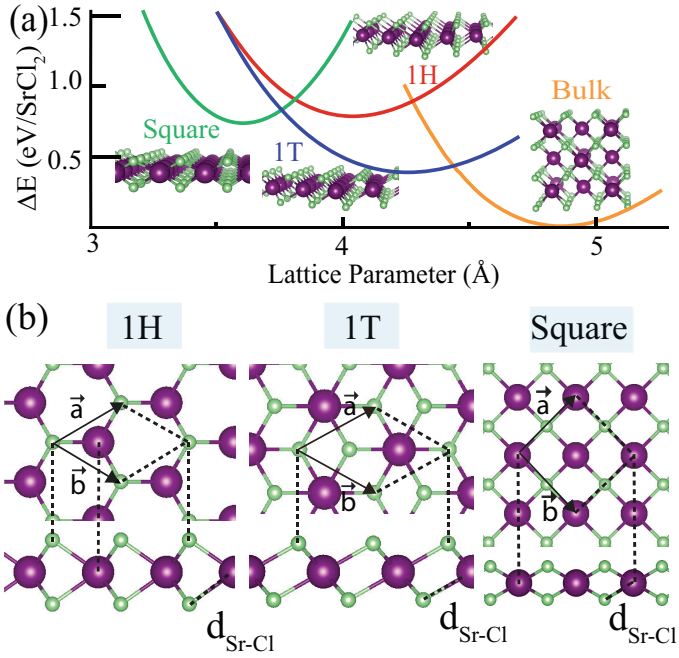


**Fig. 1** (a) Total energy differences and (b) possible crystal structures of $SrCl_2$; 1H, 1T and Square, their unit cells and lattice vectors in single-layer forms.

## 4 Dynamical, Thermal and Chemical Stability

Dynamical stability of the possible structures of $SrCl_2$ crystal structures and their characteristic Raman active phonon modes and constant volume heat capacities can be investigated through their phonon dispersions. It is seen from Figure 2 that phonon spectrum of 1H, 1T, and Square $SrCl_2$ phases is composed of 3 acoustic and 6 optical phonon branches and dynamical stability of these crystal structures can be deduced from phonon eigenfrequencies all taking real eigenvalues through the whole Brillouin zone. As a result of structural symmetry in 2D, $SrCl_2$ single-layers have 2 double-degenerate in-plane and 2 non-degenerate out-of-plane optical phonon modes at the Γ high symmetry point.

For 1H phase, analysis of the lattice dynamics shows that the decomposition of the vibration representation of optical modes at the Γ point is $\Gamma_{opt} = 2E'' + 2E' + A_1' + A_2''$. 1H structure has double-degenerate in-plane E′ (145 $cm^{-1}$) and E″ (92 $cm^{-1}$) modes and non-degenerate out-of-plane modes $A_1'$ (216 $cm^{-1}$) and $A_2''$ (223 $cm^{-1}$). Phonon eigendisplacements are shown in lower panel of Figure 2 reveal that E′, E″, and $A_1$ phonons are Raman-active lattice vibrations. In addition $A_2''$ mode shows IR activity. Similarly, 1T phase with its crystal structure that belongs to $D_{3d}$ point group has double-degenerate $E_g$ (140 $cm^{-1}$) and $E_u$ (148 $cm^{-1}$) modes and non-degenerate $A_{1g}$ (158 $cm^{-1}$) and $A_{2u}$ (198 $cm^{-1}$). However, in 1T phase, differing from 1H phase, there is a large gap between optical phonons and acoustic phonons. It is calculated

View Article Online
DOI: 10.1039/D0TC03062G



**Table 1** Calculated structural and electronic parameters of monolayer $SrCl_2$ crystals; lattice parameters of optimized 3D cubic and 2D 1H, 1T, and Square lattice ($a$), point group, bond length between adjacent atoms ($d$), total charge density donated (-) or received (+) per the atom ($\rho_{Sr}$ and $\rho_{Cl}$), energy differences of crystals ($\Delta$E), cohesive energy/$SrCl_2$ ($E_{Coh}$), work function ($\Phi$), electronic band gap with bare GGA functional ($E_{GGA}$), electronic band gap with GGA+HSE06 functional ($E_{GGA+HSE06}$), the in-plane stiffness, ($C$), Poisson ratio, ($\nu$) and Raman modes $cm^{-1}$.

| | $a$ (Å) | Point group | $d_{Sr-Cl}$ (Å) | $\rho_{Sr}$ ($e^-$) | $\rho_{Cl}$ ($e^-$) | $\triangle E$ (eV) | $E_{Coh}$ (eV) | $\Phi$ (eV) | $E_{GGA}$ (eV) | $E_{GGA+HSE06}$ (eV) | $C$ (N/m) | $\nu$ | Raman Mode $cm^{-1}$ |
|---|---|---|---|---|---|---|---|---|---|---|---|---|---|
| Bulk | 4.99 | $O_h$ | 3.05 | -1.6 | +0.8 | 0 | 3.91 | 8.51 | 5.21 | 6.55 | 44 | 0.24 | 184[59] |
| 1H | 4.18 | $D_{3h}$ | 2.94 | -1.6 | +0.8 | 0.77 | 3.14 | 7.88 | 5.08 | 6.47 | 20 | 0.47 | 92, 145, 216 |
| 1T | 4.42 | $D_{3d}$ | 2.92 | -1.6 | +0.8 | 0.38 | 3.53 | 7.74 | 5.80 | 7.19 | 20 | 0.24 | 140, 158 |
| Square | 3.70 | $D_{4h}$ | 3.08 | -1.6 | +0.8 | 0.73 | 3.18 | 7.59 | 3.70 | 5.82 | 51 | 0.05 | 61, 102, 222 |

**Table 2** Binding energies of $H_2O$, $O_2$, $CO_2$ and $N_2$ molecules on the surface of single layer $SrCl_2$.

| | $H_2O$ (meV) | $N_2$ (meV) | $O_2$ (meV) | $CO_2$ (meV) |
|---|---|---|---|---|
| 1H | 575 | 56 | 52 | 93 |
| 1T | 558 | 69 | 72 | 100 |
| Square | 538 | 62 | 67 | 122 |

that Square phase has double-degenerate E″-like (61 $cm^{-1}$) and E′-like (102 $cm^{-1}$), and nondegenerate $A_2$″-like (204 $cm^{-1}$) and $A_1$′-like (222 $cm^{-1}$) modes in its spectrum. Moreover, it is seen that in the Square phase formed by relatively weaker Sr-Cl bonds in-plane optical modes are softened with respect to 1H and 1T phase. As reported experimentally, differing from its single layer forms, the bulk form of $SrCl_2$ has only one Raman active phonon branch at 184 $cm^{-1}$.[59] Here, presence of distinctive Raman-active modes in each single layer crystal structure provides a useful recipe for experimental characterization via Raman spectroscopy. Constant volume specific heat capacities ($C_v$) of 1H, 1T, and Square $SrCl_2$ crystals are also calculated. Figure 2(d) shows that as the temperature increases, all phonon modes are stimulated and the specific heat of the structures approach the limit value of $3Nk_B$ (where N is the number of atoms per unit cell). It is also seen that dimensional reduction of bulk leads to increase in $C_v$ at low temperatures.

For examination of the thermal stability of $SrCl_2$ monolayers in 1H, 1T, and Square phases, *ab initio* MD simulations are performed from 0 to 2000 K. Figure 2(e) illustrates the average Sr-Cl bond length as a function of temperature in the MD simulations. In each phase, bond variance is negligible at low temperatures. Apparently, one can conclude that $SrCl_2$ single layers are thermally stable at room temperature. However, it is seen that, for 1H and Square phases, temperature-induced distortion in the average Sr-Cl bond length becomes significant especially over 1000 K. Here, the thermal stability of 1T phase at higher temperatures can be explained via its phonon spectrum that shows a phonon band gap of 45 $cm^{-1}$ between the acoustical and optical modes. Apparently, such decoupling prevents thermal-energy-driven simultaneous excitation of optical and acoustical modes.

Structural stability against atmospheric conditions, that directly determines the electronic and optical stability, is another important property desired for technological applications. In order to examine the chemical stability of the $SrCl_2$ single-layers, we investigate how strong is the interaction between their surface with atmosphere abundant molecules $N_2$, $O_2$, $H_2O$, and $CO_2$, see Table 2. For finding the most favorable adsorption site of the $H_2O$ molecule over the 1H, 1T and Square $SrCl_2$ total energy calculations are performed at different points on the surface. It is calculated that over the three surfaces $H_2O$ molecule strongly binds

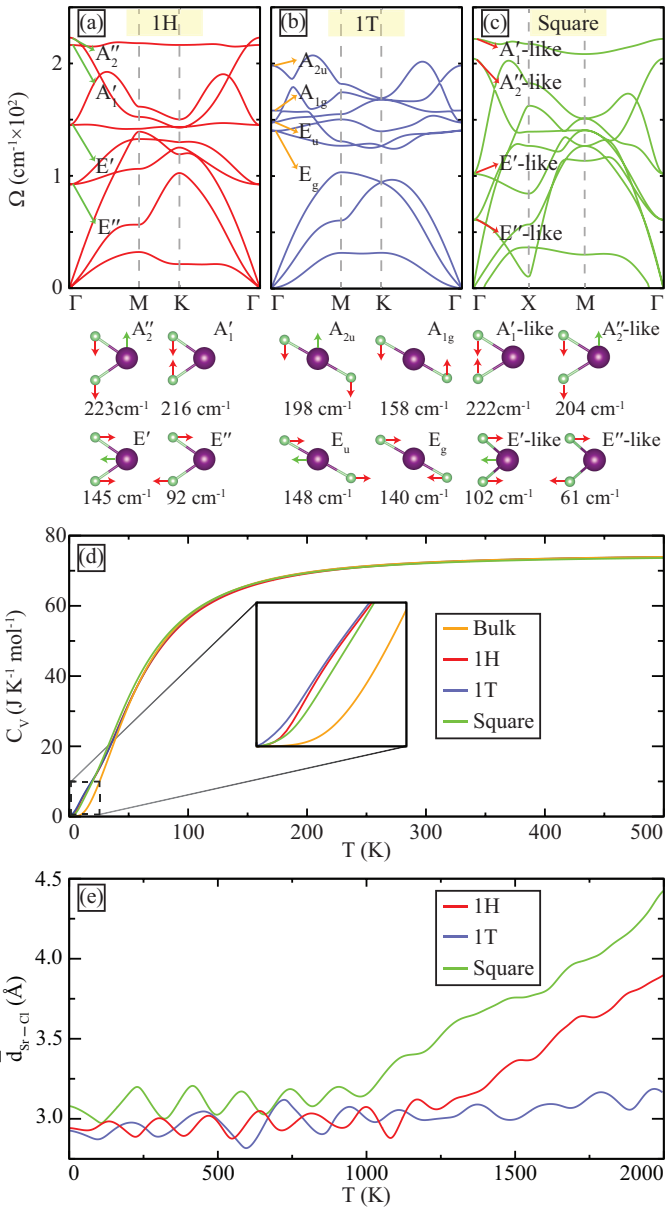


**Fig. 2** Phonon dispersions of $SrCl_2$ in (a) 1H, (b) 1T, (c) Square structure, where the insets show the vibrational modes of the corresponding phase. (d) Constant volume specific heat capacities of 1H, 1T, and square $SrCl_2$ single-layers. (e) Average Sr-Cl bond lengths of $SrCl_2$ with temperature

View Article Online
DOI: 10.1039/D0TC03062G



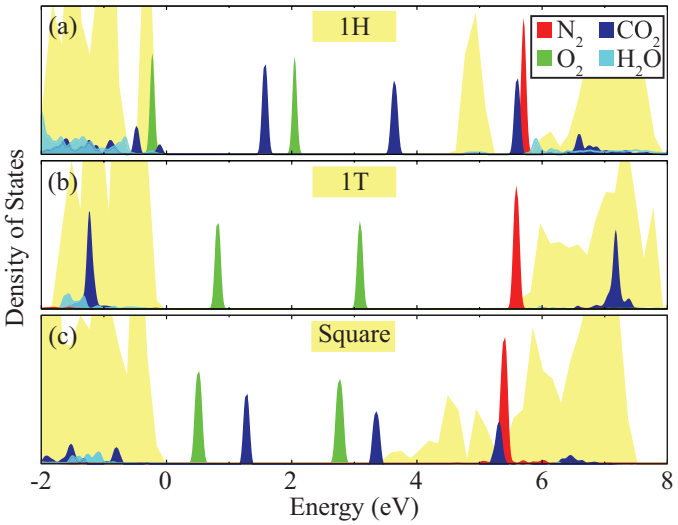


**Fig. 3** Partial density of states of $N_2$, $O_2$, $CO_2$, and $H_2O$ molecules adsorbed on (a) 1H, (b) 1T, (c) Square phases of $SrCl_2$. PDOS of $N_2$, $O_2$, $CO_2$, and $H_2O$ molecules are represented by red, green, blue, and cyan colors while $SrCl_2$ single-layers are represented by yellow color.

(between 538-575 meV) to the crystal structure with a covalent bond between Sr and O atoms. In this case Sr-O distance is found to be 2.55 Å. In addition, $N_2$ molecules weakly binds over the $SrCl_2$ single-layers, with average 3.5 Å interatomic distance with neighboring Cl atoms). The binding energies between 1H, 1T, and Square phases with $N_2$ molecule are 56, 69, and 62 meV respectively. These energy values indicate that the $N_2$ molecule has lower binding energy in the range of hydrogen type bonding. Similarly, binding energy of $O_2$ ($CO_2$ ) over 1H, 1T and Square phase crystals are found to be 52 (93), 72 (100), and 67 (122) meV, respectively. Moreover, as shown in Figure 3, partial density of states (PDOS) profile of the molecule-surface systems also provide characteristic signatures. Localized states of $N_2$, $O_2$ molecules in the PDOS agrees with the structural optimizations and binding energy calculations indicating the weak interaction between the $SrCl_2$ crystals and the molecules. On the other hand, instead of displaying localized states, $CO_2$ and $H_2O$ present coupled states with the $SrCl_2$ crystals in the PDOS. As results, $SrCl_2$ single-layers are inert against abundant molecules such as $N_2$ and $O_2$ however, they present electronic interaction with $CO_2$ and $H_2O$ molecules. Thus, it has been found that $SrCl_2$ single-layer crystals can be used to sense $CO_2$ and $H_2O$.

## 5 Electronic Properties and Possible Vertical Heterostructures

We also investigate electronic characteristics of the $SrCl_2$ single-layers through their electronic band structures. In addition to bare-GGA calculations, we perform GGA+HSE calculations to better approximate the expected experimental electronic bandgap. Therefore, bandgaps of bulk, 1H, 1T and Square $SrCl_2$, listed in Table 1, are calculated to be 5.21, 5.08, 5.80, and 3.70 eV using bare-GGA functional and 6.55, 6.47, 7.19, and 5.82 eV using the GGA+HSE hybrid functional, respectively. As seen in Figure 4, 1H phase has direct band gap with valance band maximum (VBM) and conduction band minimum (CBM) are located at M high-symmetry point, however 1T and Square type crystal structures are indirect band gap materials. Obviously, all three phases of ultra-thin $SrCl_2$ are wide band gap semiconductors as their bulk form and may find

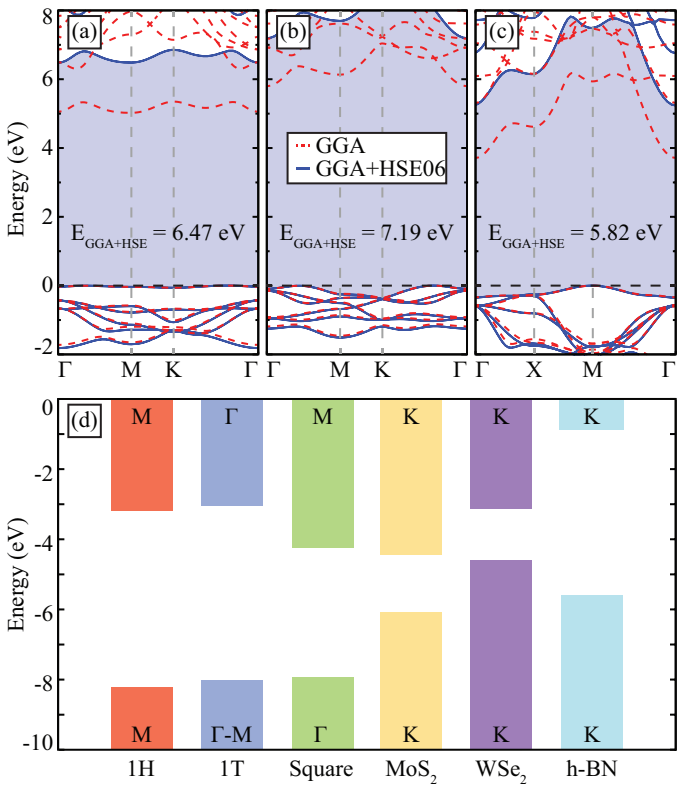


**Fig. 4** Calculated band structures of (a) 1H, (b) 1T, (c) Square phases using bare GGA and GGA+HSE functionals are presented by red, blue lines, respectively, GGA+HSE band gaps showed with blue area. (d) Comparative band alignments of 1H, 1T, and Square $SrCl_2$ phases with well-known single-layers $MoS_2$, $WSe_2$, and *h*-BN

various applications in high power electronics.[60] In addition, work functions of 1H, 1T, and Square phases are determined as 7.88, 7.74, and 7.59 eV, respectively. In comparison to the well-known single-layer materials, currently used in technology, such as $MoS_2$ (5.1 eV) or *h*-BN (4.7 eV),[61] work functions of predicted single-layer phases of $SrCl_2$ crystals are significantly higher.

Furthermore, one can deduce what type of vertical heterojunctions are formed with these ultra-thin $SrCl_2$ crystals by comparing their electronic band structures and vacuum levels. As seen in Figure 4(d), the band alignment of $SrCl_2$ single-layers are compared to well-known monolayers such as $MoS_2$, $WSe_2$, and *h*-BN by adjusting vacuum energies to zero. It is seen that vertical heterostructure of $MoS_2$ with $SrCl_2$ in 1H, 1T, and Square phases form type I heterojunction with a straddling type bandgap. On the other hand, heterostructures formed by 1H, 1T, and Square phases of $SrCl_2$ crystals with $WSe_2$ and *h*-BN are type II heterojunctions with a staggered type bandgap.

## 6 Conclusions

In this study, novel $SrCl_2$ single-layers were investigated by performing state-of-the-art first-principles calculations. In addition to total energy optimizations, phonon dispersion analysis showed that 1H, 1T, and Square phases of $SrCl_2$ are also dynamically stable crystal structures. Further investigation of their vibrational properties revealed that $SrCl_2$ single-layers have characteristic Raman active modes which enables characterization via Raman spectroscopy. Thermal stability of the $SrCl_2$ single-layers were also confirmed by MD simulations. It was also shown that 1T phase,

View Article Online
DOI: 10.1039/D0TC03062G



that displays a decoupling between acoustic and optical modes, has a better thermal stability. In addition, distinctive interactions of $SrCl_2$ single-layers with $CO_2$ and $H_2O$ can be utilized in sensing applications. Additionally, electronic structure calculations reveal that while 1H-$SrCl_2$ has a direct bandgap of 6.55 eV, 1T and Square phases have indirect bandgap of 6.47 and 7.19 eV, respectively. Due to their wide band gaps, $SrCl_2$ single-layers can be used as potential dielectric layers. It was also shown that predicted stable ultra-thin $SrCl_2$ semiconductors with their wide bandgap semiconductor behavior can form type-I and type-II van der Waals heterojunctions with well-known single layer crystals and therefore may find applications in nanoscale optoelectronics.

## Conflicts of interest

There are no conflicts to declare.

## Acknowledgements

Computational resources were provided by TUBITAK ULAKBIM, High Performance and Grid Computing Center (TR-Grid e-Infrastructure). H.S. Acknowledges financial support from the TUBITAK under the project number 117F095. H.S. acknowledges support from Turkish Academy of Sciences under the GEBIP program.

## Notes and references

1 C. Derrington, A. Lindner and M. O'keeffe, *J. Solid State Chem.*, 1975, **15**, 171–174.
2 A. Dworkin and M. Bredig, *J. of Phys. Chem.*, 1963, **67**, 697–698.
3 H. R. Rogers, C. L. Hill, Y. Fujiwara, R. J. Rogers, H. L. Mitchell and G. M. Whitesides, *J. Am. Chem. Soc.*, 1980, **102**, 217–226.
4 H. R. Rogers, R. J. Rogers, H. L. Mitchell and G. M. Whitesides, *J. Am. Chem. Soc.*, 1980, **102**, 231–238.
5 A. Vakalopoulos and H. M. R. Hoffmann, *Org. Lett.*, 2000, **2**, 1447–1450.
6 A. Bouzide, *Org. Lett.*, 2002, **4**, 1347–1350.
7 L. Sun and L. C. Chow, *Dent. Mater.*, 2008, **24**, 111–116.
8 H. H. Xu, J. L. Moreau, L. Sun and L. C. Chow, *Biomaterials*, 2008, **29**, 4261–4267.
9 A. Al-Noaman, S. C. Rawlinson and R. G. Hill, *J. Non-Cryst. Solids*, 2012, **358**, 1850–1858.
10 A. Lucca, M. Jacquemet, F. Druon, F. Balembois, P. Georges, P. Camy, J.-L. Doualan and R. Moncorgé, *Opt. Lett.*, 2004, **29**, 1879–1881.
11 M. Siebold, S. Bock, U. Schramm, B. Xu, J.-L. Doualan, P. Camy and R. Moncorgé, *Appl. Phys. B*, 2009, **97**, 327–338.
12 P. Aubry, A. Bensalah, P. Gredin, G. Patriarche, D. Vivien and M. Mortier, *Opt. Mater.*, 2009, **31**, 750–753.
13 M. S. Akchurin, T. T. Basiev, A. A. Demidenko, M. E. Doroshenko, P. P. Fedorov, E. A. Garibin, P. E. Gusev, S. V. Kuznetsov, M. A. Krutov, I. A. Mironov, V. V. Osiko and P. A. Popov, *Opt. Mater.*, 2013, **35**, 444–450.
14 Y. Y. Illarionov, A. G. Banshchikov, D. K. Polyushkin, S. Wachter, T. Knobloch, M. Thesberg, L. Mennel, M. Paur, M. Stöger-Pollach, A. Steiger-Thirsfeld, M. I. Vexler, M. Waltl, N. Sokolov, T. Mueller and T. Grasse, *Nat. Electron.*, 2019, **2**, 230–235.
15 C. Bocker, S. Bhattacharyya, T. Höche and C. Rüssel, *Acta Mater.*, 2009, **57**, 5956–5963.
16 J. Chung, Y. Watanabe, Y. Yananba, Y. Nakatsuka and H. Inoue, *J. Am. Ceram. Soc.*, 2020, **103**, 167–175.
17 D. Anderson, R. Bouclier, G. Charpak, S. Majewski and G. Kneller, *Nucl. Instrum. Meth. A*, 1983, **217**, 217–223.
18 P. Bruyndonckx, X. Liu, S. Tavernier and S. Zhang, *Nucl. Instrum. Meth. A*, 1997, **392**, 407–413.
19 A. Uchida, Y. Wakano, O. Fukuyama, T. Miki, Y. Iwayama and H. Okada, *J. Periodontol.*, 1980, **51**, 578–581.
20 S. Minkoff and S. Axelrod, *J. Periodontol.*, 1987, **58**, 470–474.
21 T. Suzuki, M. Asami, M. Hoffmann, X. Lu, M. Gužvić, C. A. Klein and A. C. Perry, *Nat. Commun.*, 2016, **7**, 1–15.
22 U. Elling, M. Woods, J. V. Forment, B. Fu, F. Yang, B. L. Ng, J. R. Vicente, D. J. Adams, B. Doe, S. P. Jackson, J. M. Penninger and G. Balmus, *Nat. Protoc.*, 2019, **14**, 1991.
23 R. Kumar and D. Fray, *Solid State Ion.*, 1988, **28**, 1688–1692.
24 K. Tang, Y. Lu, L. Jiang, A. P. Roskilly, Y. Yuan and Y. Wang, *Energy Procedia*, 2017, **142**, 4037–4043.
25 G. A. Hashmi, W. A. Syed, M. Hayat, W. H. Shah and N. A. Shah, *Mater. Res. Express*, 2019, **6**, 106440.
26 S. Wang, H. Cao, X. Liu, Y. Liu, T. Tao, J. Sun and M.-D. Zhang, *ACS Appl. Mater*, 2020, **12**, 3661–3669.
27 K. S. Novoselov, A. K. Geim, S. V. Morozov, D. Jiang, Y. Zhang, S. V. Dubonos, I. V. Grigorieva and A. A. Firsov, *Science*, 2004, **306**, 666–669.
28 A. K. Geim and K. S. Novoselov, *Nanoscience and technology: a collection of reviews from nature journals*, World Scientific, 2010, pp. 11–19.
29 A. J. Mannix, X.-F. Zhou, B. Kiraly, J. D. Wood, D. Alducin, B. D. Myers, X. Liu, B. L. Fisher, U. Santiago, J. R. Guest, M. J. Yacaman, A. Ponce, A. R. Oganov, M. C. Hersam and N. P. Guisinger, *Science*, 2015, **350**, 1513–1516.
30 C. E. Sanders, M. Dendzik, A. S. Ngankeu, A. Eich, A. Bruix, M. Bianchi, J. A. Miwa, B. Hammer, A. A. Khajetoorians and P. Hofmann, *Phys. Rev. B*, 2016, **94**, 081404.
31 Q. H. Wang, K. Kalantar-Zadeh, A. Kis, J. N. Coleman and M. S. Strano, *Nat. Nanotechnol.*, 2012, **7**, 699.
32 M. Chhowalla, H. S. Shin, G. Eda, L.-J. Li, K. P. Loh and H. Zhang, *Nat. Chem.*, 2013, **5**, 263.
33 K. F. Mak, C. Lee, J. Hone, J. Shan and T. F. Heinz, *Phys. Rev. Lett.*, 2010, **105**, 136805.
34 H. Fang, S. Chuang, T. C. Chang, K. Takei, T. Takahashi and A. Javey, *Nano Lett.*, 2012, **12**, 3788–3792.
35 S. Tongay, H. Sahin, C. Ko, A. Luce, W. Fan, K. Liu, J. Zhou, Y.-S. Huang, C.-H. Ho, J. Yan, D. F. O. Ogletree, S. Aloni, J. Ji, S. Li, J. Li, F. Peeters and J. Wu, *Nat. Commun.*, 2014, **5**, 1–6.
36 H. Sahin, S. Cahangirov, M. Topsakal, E. Bekaroglu, E. Akturk, R. T. Senger and S. Ciraci, *Phys. Rev. B*, 2009, **80**, 155453.
37 A. Molle, J. Goldberger, M. Houssa, Y. Xu, S.-C. Zhang and D. Akinwande, *Nat. Mater*, 2017, **16**, 163–169.
38 P. Vogt, P. De Padova, C. Quaresima, J. Avila, E. Frantzeskakis, M. C. Asensio, A. Resta, B. Ealet and G. Le Lay, *Phys. Rev. Lett.*, 2012, **108**, 155501.
39 M. Dávila, L. Xian, S. Cahangirov, A. Rubio and G. Le Lay, *New J. Phys.*, 2014, **16**, 095002.
40 D. Golberg, Y. Bando, Y. Huang, T. Terao, M. Mitome, C. Tang and C. Zhi, *ACS Nano*, 2010, **4**, 2979–2993.
41 K. Watanabe, T. Taniguchi and H. Kanda, *Nat. Mater.*, 2004, **3**, 404–409.
42 M. Baskurt, J. Kang and H. Sahin, *Phys. Chem. Chem. Phys.*, 2020, **22**, 2949–2954.
43 M. Baskurt, M. Yagmurcukardes, F. Peeters and H. Sahin, *J. Chem. Phys.*, 2020, **152**, 164116.
44 D. J. O'Hara, T. Zhu, A. H. Trout, A. S. Ahmed, Y. K. Luo, C. H.

View Article Online
DOI: 10.1039/D0TC03062G

Lee, M. R. Brenner, S. Rajan, J. A. Gupta, D. W. McComb and R. K. Kawakami, *Nano Lett.*, 2018, **18**, 3125–3131.
45 B. Huang, G. Clark, E. Navarro-Moratalla, D. R. Klein, R. Cheng, K. L. Seyler, D. Zhong, E. Schmidgall, M. A. McGuire, D. H. Cobden, W. Yao, D. Xiao, P. Jarillo-Herrero and X. Xu, *Nature*, 2017, **546**, 270–273.
46 W. Xing, Y. Chen, P. M. Odenthal, X. Zhang, W. Yuan, T. Su, Q. Song, T. Wang, J. Zhong, S. Jia, X. C. Xie and W. Han, *2D Mater.*, 2017, **4**, 024009.
47 T. Kong, K. Stolze, E. I. Timmons, J. Tao, D. Ni, S. Guo, Z. Yang, R. Prozorov and R. J. Cava, *Adv. Mater*, 2019, **31**, 1808074.
48 M. Baskurt, I. Eren, M. Yagmurcukardes and H. Sahin, *Appl. Surf. Sci*, 2020, **508**, 144937.
49 H. Cui, P. Jia and X. Peng, *Appl. Surf. Sci*, 2020, 145863.
50 H. Cui, C. Yan, P. Jia and W. Cao, *Appl. Surf. Sci*, 2020, **512**, 145759.
51 G. Kresse and J. Hafner, *Phys. Rev. B*, 1993, **47**, 558.
52 G. Kresse and J. Furthmüller, *Phys. Rev. B*, 1996, **54**, 11169.
53 J. P. Perdew, K. Burke and M. Ernzerhof, *Phys. Rev. Lett.*, 1996, **77**, 3865–3868.
54 P. E. Blöchl, *Phys. Rev. B*, 1994, **50**, 17953.
55 G. Henkelman, A. Arnaldsson and H. Jónsson, *Comput. Mater. Sci.*, 2006, **36**, 354–360.
56 D. Alfè, *Comput. Phys. Commun.*, 2009, **180**, 2622–2633.
57 A. Togo and I. Tanaka, *Scr. Mater.*, 2015, **108**, 1–5.
58 M. Yagmurcukardes, C. Bacaksiz, E. Unsal, B. Akbali, R. Senger and H. Sahin, *Phys. Rev. B*, 2018, **97**, 115427.
59 P. Denham, P. Morse and G. Wilkinson, *J. Phys. C Solid State Phys.*, 1973, **6**, 2066.
60 H. Zhang, H. Wang, S. T. Williams, D. Xiong, W. Zhang, C.-C. Chueh, W. Chen and A. K.-Y. Jen, *Adv. Mater.*, 2017, **29**, 1606608.
61 C. E. Dreyer, J. L. Lyons, A. Janotti and C. G. Van de Walle, *Appl. Phys. Express*, 2014, **7**, 031001.